MIP Formulation for Type-III Wind Turbines Considering Control Limits

Mohammed Alqahtani
Electrical Engineering Department
Prince Sattam Bin Abdulaziz University
Al-Kharj 16278, KSA
Email: mh.alqahtani@psau.edu.sa

Zhixin Miao
Electrical Engineering Department
University of South Florida
Tampa, FL 33620, USA
Email: zmiao@usf.edu

Lingling Fan
Electrical Engineering Department
University of South Florida
Tampa, FL 33620, USA
Email: linglingfan@usf.edu

***Abstract*—Hitting control limits changes the behavior of the control systems and invalidates commonly adopted assumptions made when calculating the operating point of doubly fed induction generator (DFIG)-based wind turbines (WTs). The current computing methods rely on trials and errors and iterations. This paper proposes an optimization-based algorithm with control limits integrated into the problem formulation. Hitting or not hitting a control limit is modeled as a binary variable. Both rotor-side converter (RSC) current order limits and grid-side converter (GSC) current order limits are modeled in the proposed mixed-integer programming (MIP) formulation. For a WT with given terminal voltage and wind speed, the electrical and mechanical variables of the system can be computed directly from the optimization problem. The proposed formulation has included losses in the back-to-back converters and nonzero reactive power support through GSC. The computing results have been validated with the electromagnetic transient (EMT) simulation results. This formulation can help accurately detect whether control limits are hit for low voltage conditions and facilitate Type-III wind turbine fault ride through analysis.**

***Index Terms*—Wind turbine, doubly-fed induction generator, model initialization, steady-state operating condition.**

I. INTRODUCTION

DFIG wind turbine (WT) a major type of WTs and design computing models for DFIG's steady-state condition characterization is of vital importance for wind farm operation. A challenge in steady-state operating condition computing is the consideration of control limits. In many operating scenarios, e.g., stator voltage dip, converters may hit the control limits. Once a limit is reached, the behavior of the WT control system changes. Considering those limits makes a computing model more sophisticated.

a) State-of-the-art review: In the literature, [1]–[4] try to tackle the challenge. The proposed methods in [1], [2] employ Newton-Raphson (NR) approach to calculate operating points of DFIG-based WTs. After each iteration, stator and rotor currents are checked for limits violations. Once a violation is identified, active and reactive power of the DFIG are recalculated using the PQ curve proposed in [5] which ignores the converters and machine active losses. Moreover, only zero reactive power support through GSC is considered.

This work is supported in part by NSF grant 2103480 "Dynamic Model Identification for Inverter-Based Resources".

In [3], [4], for short circuit studies, a Type-III WT is modeled as a voltage-dependant current source and incorporated in an iterative process. In [3], rotor current limits are taken into consideration. The proposed method in [3] has been improved in [4] by considering the grid-side converter limits and the unbalanced stator condition. However, both methods assume a constant rotor speed and lossless converters. Furthermore, the above research ignores the active losses in the induction machine.

b) Contributions: The goal of this paper is to construct an *efficient and accurate* computing model for DFIG steady-state calculation with control limits considered. Moreover, we aim to improve the way that control limits are being handled by proposing a one-step algorithm through optimization problem formulation. As comparison, the state-of-the-art methods mentioned above all require multiple stages.

Our contribution is the formulation of a mixed-integer nonlinear programming (MINLP) problem for DFIG steady-state calculation. In this formulation, the fundamental laws of a circuit, e.g., current, voltage and power relationships, are expressed as equality constraints. The proportional integral control functions employed in current controls of the rotor-side converters (RSCs) and the grid-side converters (GSCs) are expressed as either equality constraints or relaxed when the current order limits are hit. Whether a control limit is hit or not is modeled as a binary variable. Both RSC and GSC control limits are considered and the resulting MINLP problem is solved by use of YALMIP's BMIBNB solver [6].

c) Structure: This paper starts with a brief presentation of a Type-III WT and its control system in section II. Section III presents the steady-state model of the system. The optimization problem formulation is presented in section IV. Section V verifies the proposed approach through electromagnetic transient (EMT) simulation results. Section VI concludes the paper.

II. TYPE-III WTS

The typical configuration of a DFIG-based WT is shown in Fig. 1. The stator of the induction machine (IM) is directly connected to the grid, and the rotor is connected to the grid through a back-to-back converter. The back-to-back converter consists of two three-phase converters: RSC and GSC. The

978-1-6654-9921-7/22/$31.00 ©2022 IEEE

GSC is connected to the grid through a filter. The two converters are coupled through a common DC link. The symbols have been explained in the caption of Fig. 1.

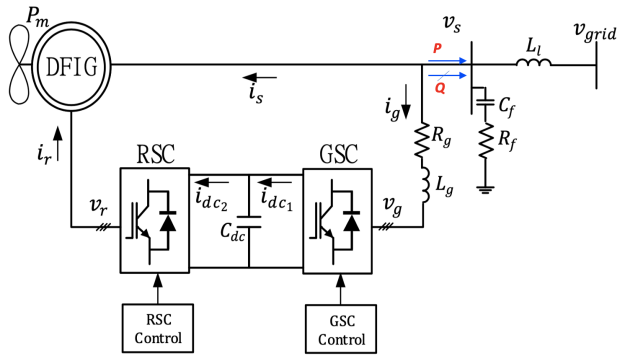

Fig. 1: System configuration.i_s, i_r and i_g are the DFIG stator, rotor, and grid-side converter currents, respectively. v_s, v_r and v_g are terminal voltages of the DFIG stator, rotor, and grid side-converter. P and Q are the DFIG-base WT real and reactive power outputs. R_g and X_g are the resistance and reactance of the DFIG back-to-back converter. C_{dc} is the DC-link capacitance of the DIFG back-to-back converter. P_m is the mechanical power.

A. Control System

The RSC control system implemented is shown in Fig. 2a. $i_{\rm dr}, i_{\rm qr}, v_{\rm dr}, v_{\rm qr}$ are the DFIG rotor currents and voltages on the d and q axes, respectively. θ_m is the rotor mechanical angle, and θ_e is the rotor electrical angle.

The control of RSC is achieved using a two-level controller: fast inner loops and slow outer loops. The inner loops are used to calculate the voltage references in order to generate the modulation index. The slow outer loops are used to calculate the current references $i^{*'}_{\rm dr}, i^{*'}_{\rm qr}$. In the given control system, the outer loops regulate the electromagnetic torque ($T_{\rm em}$) and the stator reactive power (Q_s). The two controls are implemented by referring all AC quantities to a synchronous reference frame oriented with the stator voltage as adopted in [7]: $v_{\rm ds} = |\overline{V_s}|$ and $v_{\rm qs} = 0$.

A similar technique is used for the GSC controls, as shown in Fig. 2b. $i_{\rm dg}, i_{\rm qg}, v_{\rm dg}, v_{\rm qg}$ are grid-side-converter currents and voltages on the d and q axes, respectively. The outer loops of the control regulate the DC-link capacitor voltage (V_{dc}) and reactive power (Q_g).

B. Low-voltage ride through (LVRT) function

When the stator voltage is below a certain value ($V_{\rm LVRT}$), the behavior of the control system of RSC changes with the LVRT activated. The Q-control will be deactivated, and the WT will generate a reactive current component proportional to the voltage drop.

It should be noted that the LVRT function is essential for the WTs operating under the Q-control to comply with the grid code requirements regarding the voltage support. During that mode, the reactive current reference is calculated based on equation (1). A similar control scheme (LVRT function) has been adopted in [3], [8]–[12]. This control is referred to

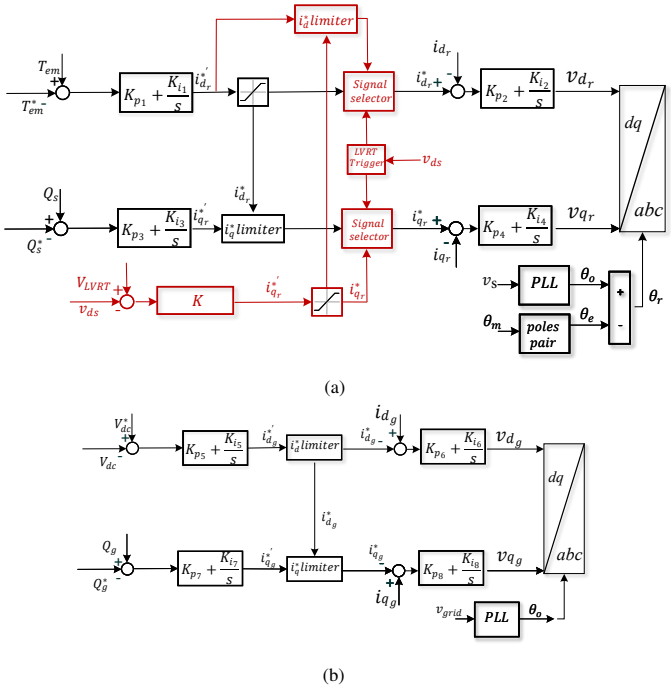

Fig. 2: (a) RSC Control. (b) GSC control.

"k-factor control" for a WT to provide reactive power upon voltage dip.

$$i^*_{qr} = K(V_{\rm LVRT} - v_{ds}) \tag{1}$$

where K is the proportional gain and K is negative. Note that v_{ds} is viewed as the stator voltage's magnitude. The dq-frame is aligned to the stator voltage through a phase-locked-loop (PLL). Hence the d-axis stator voltage reflects the stator voltage magnitude. If the sensed voltage magnitude is below a threshold, e.g., 0.90 p.u., the WT's q-axis current order will decrease. In turn, the reactive power from the WT will increase.

C. Converters Current Limits

In order to avoid overcurrent scenarios that may damage the converters, current limiters are imposed. The control system should be able to track the outer loop references as long as the current limits are not reached. Once the limits are hit, following the references is not guaranteed. For a grid-connected DFIG, scenarios where converters hit the limits may occur. During such scenarios, the control system should give priority to either the active or reactive power. The control system will try to keep the prioritized quantity unchanged. The un-prioritized quantity will be changed, and it will not follow the reference value due to the current limits.

In this paper, the RSC and GSC current limiters give priority to the active currents or the d-axis current based on (2)-(5). When the LVRT mode is activated, the priority for the RSC is switched from the active to the reactive current. The controller is then switched from the Q-control to a proportional V-control

to fulfill the grid code requirement regarding voltage support during voltage disturbances.

$$i^*_{\mathrm{dr}} = \begin{cases} i^{*'}_{\mathrm{dr}}, & \text{if } -I_r^{\mathrm{limit}} \le i^{*'}_{\mathrm{dr}} \le I_r^{\mathrm{limit}} \\ I_r^{\mathrm{limit}}, & \text{if } I_r^{\mathrm{limit}} < i^{*'}_{\mathrm{dr}} \\ -I_r^{\mathrm{limit}}, & \text{if } -I_r^{\mathrm{limit}} > i^{*'}_{\mathrm{dr}} \end{cases} \tag{2}$$

$$i^*_{\mathrm{qr}} = \begin{cases} i^{*'}_{\mathrm{qr}}, & \text{if } \sqrt{i^{*2}_{\mathrm{dr}} + i^{*'2}_{\mathrm{qr}}} \le I_r^{\mathrm{limit}} \\ \sqrt{I_r^{\mathrm{limit}} - i^{*2}_{\mathrm{dr}}} & \text{if } \sqrt{i^{*2}_{\mathrm{dr}} + i^{*'2}_{\mathrm{qr}}} > I_r^{\mathrm{limit}}, i^{*'}_{\mathrm{qr}} > 0 \\ -\sqrt{I_r^{\mathrm{limit}} - i^{*2}_{\mathrm{dr}}} & \text{if } \sqrt{i^{*2}_{\mathrm{dr}} + i^{*'2}_{\mathrm{qr}}} > I_r^{\mathrm{limit}}, i^{*'}_{\mathrm{qr}} < 0 \end{cases} \tag{3}$$

$$i^*_{\mathrm{dg}} = \begin{cases} i^{*'}_{\mathrm{dg}}, & \text{if } -I_g^{\mathrm{limit}} \le i^{*'}_{\mathrm{dg}} \le I_g^{\mathrm{limit}} \\ I_g^{\mathrm{limit}}, & \text{if } I_g^{\mathrm{limit}} < i^{*'}_{\mathrm{dg}} \\ -I_g^{\mathrm{limit}}, & \text{if } -I_g^{\mathrm{limit}} > i^{*'}_{\mathrm{dg}} \end{cases} \tag{4}$$

$$i^*_{\mathrm{qg}} = \begin{cases} i^{*'}_{\mathrm{qg}}, & \text{if } \sqrt{i^{*2}_{\mathrm{dg}} + i^{*'2}_{\mathrm{qg}}} \le I_g^{\mathrm{limit}} \\ \sqrt{I_g^{\mathrm{limit}} - i^{*2}_{\mathrm{dg}}} & \text{if } \sqrt{i^{*2}_{\mathrm{dg}} + i^{*'2}_{\mathrm{qg}}} > I_g^{\mathrm{limit}}, i^{*'}_{\mathrm{qg}} > 0 \\ -\sqrt{I_g^{\mathrm{limit}} - i^{*2}_{\mathrm{dg}}} & \text{if } \sqrt{i^{*2}_{\mathrm{dg}} + i^{*'2}_{\mathrm{qg}}} > I_g^{\mathrm{limit}}, i^{*'}_{\mathrm{qg}} < 0 \end{cases} \tag{5}$$

III. Steady-State DFIG WT Model

At steady-state, the electrical equivalent circuit of the DFIG in dq-frame (shown in Fig 3) can be expressed by the following equations.

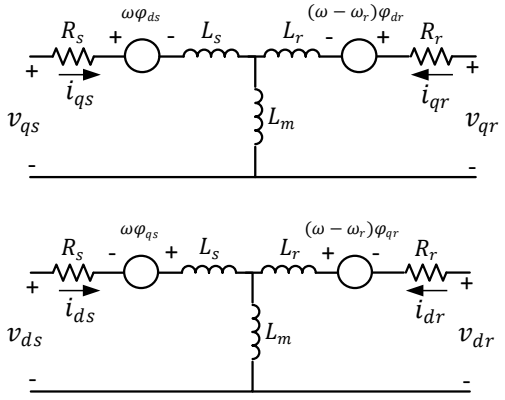

Fig. 3: Equivalent circuit of the DFIG. (a) q axis. (b) d axis.

$$v_{qs} - R_s i_{qs} - (X_s + X_m) i_{ds} - X_m i_{dr} = 0 \tag{6a}$$
$$v_{ds} + (X_s + X_m) i_{qs} - R_s i_{ds} + X_m i_{qr} = 0 \tag{6b}$$
$$v_{qr} - s X_m i_{ds} - R_r i_{qr} - s(X_r + X_m) i_{dr} = 0 \tag{6c}$$
$$v_{dr} + s X_m i_{qs} + s(X_r + X_m) i_{qr} - R_r i_{dr} = 0 \tag{6d}$$

R_s, R_r are resistance and reactance of DFIG rotor and stator circuits, respectively. X_s, X_r are reactance of DFIG rotor and stator circuits, respectively. X_m DFIG mutual reactance. s is the slip.

According to the power conservation theorem, the mechanical power, which is the power extracted from the wind by the WT, is equal to the sum of rotor and stator active power and losses. The power balance equations can be written in terms of the electrical variables as the following.

$$-P - i_{dg}^2 R_g - i_{qg}^2 R_g - i_{ds}^2 R_s - i_{qs}^2 R_s - i_{dr}^2 R_r - i_{qr}^2 R_r + P_m = 0 \tag{7a}$$
$$P + \underbrace{v_{ds} i_{ds} + v_{qs} i_{qs}}_{P_s} + \underbrace{v_{ds} i_{dg} + v_{qs} i_{qg}}_{P_g} = 0 \tag{7b}$$
$$k_p C_p W_{\mathrm{wind}}^3 - P_m = 0 \tag{7c}$$

W_{wind} is wind speed in per unit of the base wind speed. c_p is performance coefficient in per unit. k_p is the power gain for $c_p = 1$ pu and $W_{\mathrm{wind}} = 1$ pu.

The dynamics of the DC-link between the rotor and grid side converter can be represented by the following equation.

$$\begin{aligned} C_{dc} v_{dc} \frac{dv_{dc}}{dt} &= P_g - P_r - R_g I_g^2 \\ \text{where} \quad P_g &= v_{qs} i_{qg} + v_{ds} i_{dg} \\ P_r &= v_{qr} i_{qr} + v_{dr} i_{dr} \end{aligned} \tag{8}$$

At steady-state and three-phase balanced condition, the equation in (8) can be rewritten as the following considering the active losses of the GSC.

$$P_g - P_r = R_g (i_{dg}^2 + i_{qg}^2). \tag{9}$$

The control scheme of the RSC is set to regulate the electromagnetic torque and reactive power. At nominal steady-state operating condition, the following equations are satisfied.

$$\underbrace{X_m (i_{qs} i_{dr} - i_{ds} i_{qr})}_{T_{em}} - T^*_{em} = 0 \tag{10a}$$
$$\underbrace{-v_{ds} i_{qs}}_{Q_s} - Q^*_s = 0 \tag{10b}$$

When the rotor current hits the limit ($\sqrt{i^2_{\mathrm{dr}} + i^2_{\mathrm{qr}}} = I_r^{\mathrm{limit}}$), the above two equality constraints are not always true. Rather,

$$T_{em} - T^*_{em} = \mathrm{error}_1, \;\; Q_s - Q^*_s = \mathrm{error}_2. \tag{11}$$

Furthermore, if the LVRT mode is activated, the RSC controller will target satisfying equation (1) to comply with the grid code requirement.

The GSC control behaves similarly to regulate the DC-link voltage and reactive power. However, when the active current reaches the limit the dc-bus voltage rises rapidly unless a DC-link chopper is used.

IV. MINLP Problem Formulation

The main challenge in finding the steady-state variable of the DFIG-based WT is identifying the operating mode of the control systems. At normal operation conditions, it can be easy to determine the operating mode of the control system as no limits are being hit. It is usually assumed that the control system is able to track the reference values. However, during voltage dip, for instance, it is not known whether a limit is

being reached or not. It is also not known which converter reaches its limits.

For a given stator voltage, there are multiple possibilities that can be considered as shown in Fig. 4. Depending on the settings of the RSC and GSC controllers and the magnitude of the stator voltage, the control system of Type-III WT may operate at one of these possible operating modes.

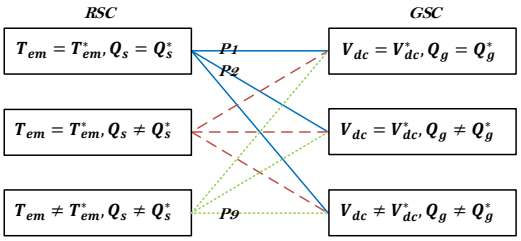

Fig. 4: Possible operating conditions.

A. Control system modeling

The control system of Type-III WTs will always aim to minimize the absolute error between the actual and reference values of the outer loops. It will always seek zero error. However, the current limiters may prevent that. If the LVRT function and the priority of active current are neglected at this stage, the behavior of the RSC control system can be modeled with the following optimization problem.

$$\begin{aligned} \text{minimize} \quad & |Q_s - Q^*_s| + |T_{em} - T^*_{em}| \\ \text{subject to} \quad & i_{qr}^2 + i_{qr}^2 \leq \left(I_r^{\text{limit}}\right)^2 \end{aligned}$$

The effect of the outer loops is incorporated in the objective function while the current limiters behavior is incorporated as an inequality constraint.

1) Active current priority modeling: The previous formulation does not differentiate between the prioritized (T_{em}) and the un-prioritized (Q_{em}) quantities as they are both incorporated equally in the objective function. Naturally, one may think to multiply the prioritized quantity with a very high penalty coefficient. However, that formulation tends to be weak as the penalty coefficient value affects the solution. Too large will affect the efficiency of the calculation and the optimal solution will not always be obtained, and a small value will not achieve the goal and will not prioritize T^*_{em} over Q^*_s.

Alternatively, the equation related to the prioritized quantity can be inserted as an equality constraint while the un-prioritized quantity is kept in the objective function. By doing so, we ensure that the prioritized quantity is met first.

However, there is a region where the control system can not track the prioritized quantity. To overcome that issue, a binary variable (u_1) is used.

$$u_1 = \begin{cases} 0, & (i_{dr})^2 < (I_r^{\text{limit}})^2, \text{limit not hitting} \\ 1, & (i_{dr})^2 = (I_r^{\text{limit}})^2, \text{ limit hitting} \end{cases} \tag{13}$$

When $u_1 = 1$, T_{em} can no longer track its reference T^*_{em}, i_{dr} assumes the limit value while i_{qr} assumes 0. When $u_1 = 0$, T_{em} tracks its reference T^*_{em} and the other two constraints are relaxed.

The above logic can be modeled as a set of constraints with u_1 incorporated.

$$\begin{aligned} \text{minimize} \quad & |Q_s - Q^*_s| + |T_{em} - T^*_{em}|u_1 \\ \text{subject to} \quad & (T_{em} - T^*_{em})(1 - u_1) = 0 \\ & i_{qr}u_1 = 0 \\ & u_1 I_r^{\text{limit}^2} \leq i_{dr}^2 \leq I_r^{\text{limit}^2},\ i_{qr}^2 + i_{qr}^2 \leq I_r^{\text{limit}^2} \end{aligned}$$

2) LVRT considered: When the adopted LVRT function is activated, the priority in the RSC is switched from the active to the reactive current, and the controller is switched from the Q-control to a proportional V-control.

To incorporate that effect into the MIP formulation in the previous section, a binary variable u_2 is considered.

$$u_2 = \begin{cases} 0, & V_s \geq V_{LVRT}, \text{ LVRT not enabled} \\ 1, & V_s < V_{LVRT}, \text{ LVRT enabled} \end{cases} \tag{14}$$

The LVRT constraint in (1) is added as an equality constraint.

$$u_2(K(V_{\text{LVRT}} - v_{ds}) - i_{qr}) = 0 \tag{15}$$

When $u_2 = 0$, this constraint is relaxed.

B. Overall MINLP formulation

The overall MINLP formulation for calculating the steady-state variables of Type-III WTs considering the both the RSC and GSC control system behavior is the following:

$$\begin{aligned} \text{minimize} \quad & |Q_s - Q^*_s|(1 - u_2) + |Q_g - Q^*_g| \\ & + |T_{em} - T^*_{em}|(u_1 + u_2) \\ \text{subject to} \quad & (6-7), (9) \\ & (T_{em} - T^*_{em})(1 - u_1)(1 - u_2) = 0 \\ & u_2(K(V_{\text{LVRT}} - v_{ds}) - i_{qr}) = 0 \\ & u_2 + u_1 \leq 1,\ i_{qr}u_1 = 0 \\ & u_1 I_r^{\text{limit}^2} \leq i_{dr}^2 \leq I_r^{\text{limit}^2} \\ & i_{qr}^2 + i_{qr}^2 \leq I_r^{\text{limit}^2},\ i_{qg}^2 + i_{qg}^2 \leq I_g^{\text{limit}^2} \\ & -0.5 \leq s \leq 0.5 \end{aligned}$$

The objective function of the optimization problem is the minimization of the absolute error of the control system equations except the DC-Link voltage.

The constraints of the optimization problem include the steady-state circuit and power equations. The behavior of the current limiters is incorporated in the optimization problem using equality and inequality constraints. The decision variables are the stator currents, rotor currents, grid side converter currents, rotor voltages, DFIG active power, DFIG mechanical power, slip and one of the two binary variables. ($i_{\text{ds}}, i_{\text{qs}}, i_{\text{dr}}, i_{\text{qr}}, i_{\text{dg}}, i_{\text{qg}}, v_{\text{dr}}, v_{\text{qr}}, P, P_m, s, u_1$). The inputs of the optimization problem are the stator voltage and wind speed. Since the stator voltage is given, u_2 is also treated as given.

As a total, there are 12 decision variables. If u_1 is not considered and all control limits are not hit, the 11 decision

variables can be found using 11 equality constraints. (6), (7), (9), (10) provide a total of 10 equality constraints. The 11th is provided from the GSC Q-following control that $Q_g = Q_g^*$.

V. Validation

To validate the analysis conducted in the previous section, a testbed of Type-III WTs model is simulated in MATLAB/SimPowerSystems(2020). Table I presents the detailed parameters of the EMT model.

TABLE I: Parameters of Simulink model

R_s	0.023(p.u)	friction factor	0	X_g	0.3(p.u)
R_r	0.016(p.u)	pole pairs	3	R_g	0.003(p.u)
X_s	0.18(p.u)	Inertia	0.0685 s	C_{dc}	0.01 (F)
X_r	0.16(p.u)	S_n	1.5 (MVA)	V_{dc}	1150 V
X_m	2.9(p.u)	V_n	575 V	Q_s^*	-0.2(p.u)
I_r^{limit}	1(p.u)	I_g^{limit}	0.5(p.u)	Q_g^*	-0.4(p.u)
W_{wind}	$11\,m/s$ (1 p.u)	T_{em}^*	-0.70(p.u)	f_n	60 Hz

In this section, the case studies are chosen such that the effectiveness of the proposed algorithm in handling various limits of DFIG can be demonstrated. The calculations are conducted considering five different values of the stator voltages, which lead to different operating modes of the control systems. In Case-A, the stator voltage is equal to 1 p.u, so the system is operating normally. In Case-B, the stator voltage is dropped to 0.80 p.u, so the RSC controller can not track the reactive power reference. In Case-C, the stator voltage is dropped to 0.75 p.u, so the GSC and RSC controllers can not track the reactive power references. In Case-D, the stator voltage is dropped to 0.72 p.u, so the GSC controllers can not track the reactive power reference. The RSC controller can not track the electromagnetic and reactive power references at that voltage level. In Case-E, the stator voltage is dropped to 0.65 p.u, so the LVRT function is activated. The RSC controller give priority to the reactive current to follow the LVRT requirement ($i_{qr}^* = K(V_{\text{LVRT}} - v_{ds})$. As a result, the RSC controller can not track the electromagnetic torque reference.

The steady-state calculations are conducted using YALMIP [6]. The formulated MIP problem is solved using `BMIBNB` (a built in solver on YALMIP). The solver implements a standard branch and bound algorithm. The solver relies on external linear, quadratic and semidefinite programming solvers for solving the lower bounding relaxation problems, and nonlinear solvers for the upper bound computations (`FILTERSD`). It also uses an external linear programming solver for bound strengthening (`GLPK`).

The results obtained from the steady-state calculation problem are shown in Table II. The mismatch between the EMT results and the calculation results is shown in Table III. Fig. 5 presents EMT simulation results for a voltage dip case. The calculated results are also plotted in dotted lines to provide a comparison. It can be seen that the proposed formulation can accurately match the EMT simulation results at steady state.

VI. Conclusion

In this article, a MINLP formulation is introduced to accurately model Type-III considering the behavior of the control system. Through optimization problem formulating and solving, the steady-state operating point of Type-III can be determined accurately. The electrical and mechanical variables of the system can be calculated for a given stator voltage and wind speed. Certain simplifying assumptions that are frequently made in the literature are avoided. Losses in the back-to-back converter are considered, as is the non-zero reactive power support provided by the GSC. The analysis results have been benchmarked with EMT simulation results. In comparison with state-of-the-art, the proposed methods result in a more efficient and accurate Type-III computation model. Advanced computing technology relying on readily available open-source solvers has been used in this research.

TABLE II: Proposed method results

	Case-A	Case-B	Case-C	Case-D	Case-E
v_{dr}	-0.0125	-0.0048	-0.0017	-0.0029	-0.1700
v_{qr}	-0.0140	-0.0130	-0.0109	-0.0091	-0.0828
i_{ds}	-0.6882	-0.8535	-0.9080	-0.9398	-0.8911
i_{qs}	0.2000	0.1335	-0.0014	-0.2408	0.0883
i_{dg}	-0.0007	0.0024	0.0026	-0.0030	-0.2047
i_{qg}	0.4000	0.5000	0.5000	0.5000	0.4562
i_{dr}	0.7293	0.9055	0.9644	1.0000	0.9457
i_{qr}	-0.5627	-0.4244	-0.2644	0	-0.3250
P_m	0.7148	0.7148	0.7148	0.7172	0.7475
P	0.6889	0.6809	0.6791	0.6788	0.7123
s	-0.0211	-0.0211	-0.0211	-0.0271	-0.2507

TABLE III: Steady-state mismatch

	Case-A	Case-B	Case-C	Case-D	Case-E
v_{dr}	-0.25×10^{-4}	-0.21×10^{-5}	-0.26×10^{-5}	-0.09×10^{-4}	0.02×10^{-6}
v_{qr}	-0.05×10^{-4}	-0.07×10^{-5}	-0.10×10^{-5}	-0.04×10^{-4}	0.04×10^{-6}
i_{ds}	-0.01×10^{-5}	-0.02×10^{-6}	-0.02×10^{-6}	0.09×10^{-5}	-0.01×10^{-6}
i_{qs}	-0.01×10^{-5}	-0.05×10^{-5}	-0.11×10^{-5}	0.04×10^{-5}	-0.10×10^{-6}
i_{dg}	-0.15×10^{-4}	-0.21×10^{-5}	-0.30×10^{-5}	-0.12×10^{-4}	0.01×10^{-6}
i_{qg}	0.01×10^{-5}	-0.01×10^{-5}	-0.01×10^{-5}	-0.07×10^{-5}	0.01×10^{-6}
i_{dr}	0.01×10^{-5}	0.02×10^{-6}	0.031×10^{-6}	-0.09×10^{-5}	0.01×10^{-6}
i_{qr}	0.01×10^{-5}	0.05×10^{-5}	0.11×10^{-5}	-0.04×10^{-5}	0.06×10^{-7}
P_m	0.12×10^{-4}	0.13×10^{-5}	0.18×10^{-5}	0.06×10^{-4}	0.02×10^{-6}
P	0.15×10^{-4}	0.17×10^{-5}	0.22×10^{-5}	0.08×10^{-4}	-0.04×10^{-8}
s	-0.22×10^{-4}	-0.24×10^{-5}	-0.32×10^{-5}	-0.13×10^{-4}	0.60×10^{-6}

References

[1] S. S. K. V. and D. Thukaram, "Accurate modeling of doubly fed induction generator based wind farms in load flow analysis," *Electric Power Systems Research*, vol. 155, pp. 363 – 371, 2018. [Online]. Available: http://www.sciencedirect.com/science/article/pii/S0378779617303784

[2] A. CVS, "Enhanced modelling of doubly fed induction generator in load flow analysis of distribution systems," *IET Renewable Power Generation*, vol. 15, no. 5, pp. 980–989, 2021.

[3] T. Kauffmann, U. Karaagac, I. Kocar, H. Gras, J. Mahseredjian, B. Cetindag, and E. Farantatos, "Phasor domain modeling of type iii wind turbine generator for protection studies," in *2015 IEEE Power & Energy Society General Meeting*. IEEE, 2015, pp. 1–5.

[4] T. Kauffmann, U. Karaagac, I. Kocar, S. Jensen, J. Mahseredjian, and E. Farantatos, "An accurate type iii wind turbine generator short circuit model for protection applications," *IEEE Transactions on Power Delivery*, vol. 32, no. 6, pp. 2370–2379, 2017.

[5] T. Lund, P. Sørensen, and J. Eek, "Reactive power capability of a wind turbine with doubly fed induction generator," *Wind Energy: An International Journal for Progress and Applications in Wind Power Conversion Technology*, vol. 10, no. 4, pp. 379–394, 2007.

[6] J. Lofberg, "Yalmip: A toolbox for modeling and optimization in matlab," in *2004 IEEE international conference on robotics and automation (IEEE Cat. No. 04CH37508)*. IEEE, 2004, pp. 284–289.

[7] S. Muller, M. Deicke, and R. W. De Doncker, "Doubly fed induction generator systems for wind turbines," *IEEE Industry applications magazine*, vol. 8, no. 3, pp. 26–33, 2002.

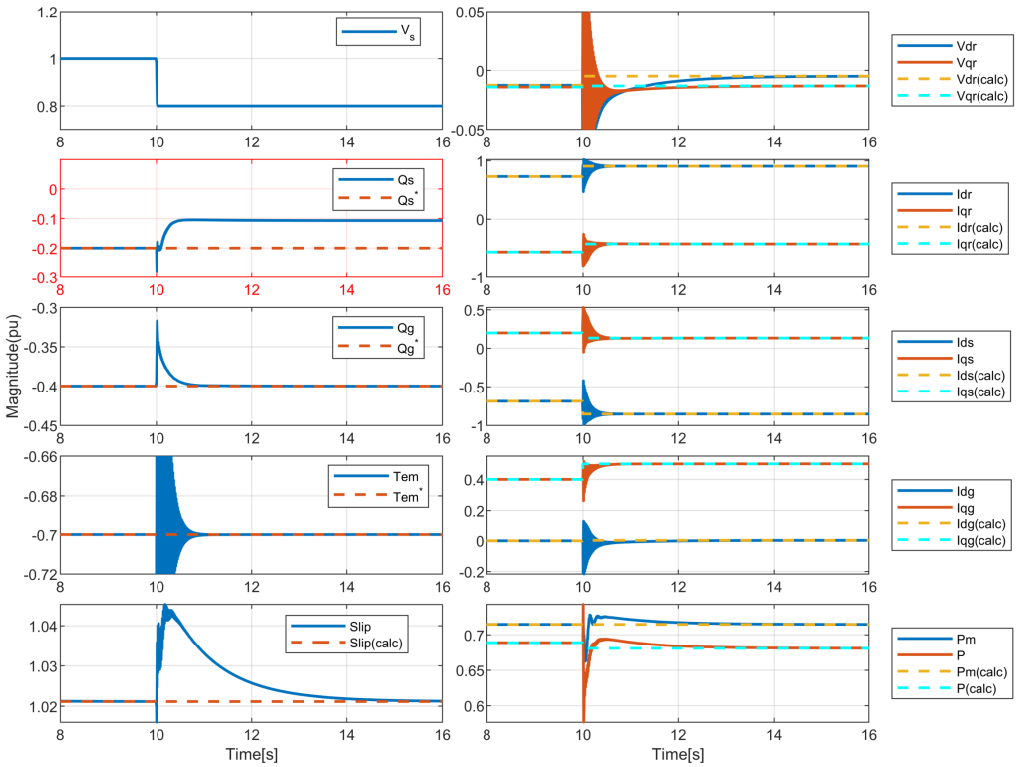

Fig. 5: Comparison between the simulation and proposed method results at two operation points. The calculation can match the simulation results very well. When $t < 10$, the current limits are not reached, so the control systems track the references, e.g., the stator reactive power operates at the reference order -0.2 pu. When $t > 10$, the reactive power of the WT increases due to k-factor control.

[8] E. Netz, "Grid code—high and extra high voltage. e. on netz gmbh," Tech. Rep.[Online]. Available: http://www. eonnetz. com/Ressources/downloads ..., Tech. Rep., 2006.

[9] T. Kauffmann, U. Karaagac, I. Kocar, S. Jensen, J. Mahseredjian, and E. Farantatos, "An accurate type iii wind turbine generator short circuit model for protection applications," *IEEE Transactions on Power Delivery*, vol. 32, no. 6, pp. 2370–2379, 2016.

[10] U. Karaagac, T. Kauffmann, I. Kocar, H. Gras, J. Mahseredjian, B. Cetindag, and E. Farantatos, "Phasor domain modeling of type-iv wind turbine generator for protection studies," in *2015 IEEE Power Energy Society General Meeting*, 2015, pp. 1–5.

[11] T. Kauffmann, U. Karaagac, I. Kocar, S. Jensen, E. Farantatos, A. Haddadi, and J. Mahseredjian, "Short-circuit model for type-iv wind turbine generators with decoupled sequence control," *IEEE Transactions on Power Delivery*, vol. 34, no. 5, pp. 1998–2007, 2019.

[12] O. Goksu, R. Teodorescu, B. Bak-Jensen, F. Iov, and P. C. Kjaer, "An iterative approach for symmetrical and asymmetrical short-circuit calculations with converter-based connected renewable energy sources. application to wind power," in *2012 IEEE Power and Energy Society General Meeting*, 2012, pp. 1–8.